Progress In Electromagnetics Research M, Vol. 104, 91–100, 2021

The Application of Artificial Magnetic Conductors in the Broadband Radar Cross Section Reduction of the Microstrip Antenna Array

Ping Yang[1], Jinbo Liu[2], and Zengrui Li[2, *]

Abstract—A scheme for radar cross section (RCS) reduction of microstrip antenna array in wideband using artificial magnetic conductors (AMC), without compromising the radiation characteristics of the antenna array, is proposed. This design is based on the principle of passive cancelation. The novelty is that the reflection characteristics of the microstrip antenna array are also taken into consideration during the design process of AMCs. The aperiodic configuration is composed of three kinds of AMC lattices with selected dimensions and is applied to the design of microstrip antenna array for the purpose of RCS reduction. The simulated results show that the monostatic RCS is reduced over a wideband from 15.2 to 35 GHz (about 79% relative bandwidth), covering the operation band (20–20.75 GHz) of the antenna array. In addition, compared with the periodic configuration, it has about 4 dB lower maximum bistatic RCS.

1. INTRODUCTION

Antennas remarkably contribute to the overall radar cross section (RCS) signature of stealth targets. Researches about RCS reduction of antennas are therefore of extensive interest. Many novel techniques have been proposed for the RCS reduction of antennas, such as the application of frequency selective surface (FSS) [1–3], artificial magnetic conductor (AMC) [4–7], and polarization conversion material (PCM) [8, 9]. However, not all of them are suitable for the RCS reduction of antennas because it may significantly affect the radiation characteristics of the antenna. In [1], the solid ground plane of the antenna is replaced by a suitable FSS. The proposed design decreases the out-of-band radar signature of the target and does not affect the in-band performance of the radiation device. For the case of reducing RCS of antennas in wide angular range, a polarization-dependent FSS (PDFSS) structure is utilized [2]. RCS reduction can be achieved in the angular range of -90° to 90° in both the E and H planes while the radiation characteristics are maintained. However, the RCS reduction band is narrow. To expand the reduction band, a band stop square loop FSS is applied as the ground plane [3]. The stopband of the FSS is the same as the working band of antenna, so that the FSS acts as the ground plane in the stopband and is transparent to the incident waves in the other frequencies. A combination of AMCs and perfect electric conductor cells is used to realize RCS reduction in a narrow band [4]. Due to the 180° phase shift generated between reflected waves, energy can be canceled out in the specular direction. However, this structure is limited by a narrow bandwidth. A chessboard configuration consisting of two different AMCs is employed for achieving a broadband RCS reduction over 60% [5, 6]. In [7], a one-dimensional metasurface based on size-adjustable meta-atoms is designed for ultra-wideband specular reflection reduction. Applications based on the mechanism of polarization rotation, which are obtained by polarization conversion material (PCM), are presented in [8, 9]. The main advantage of this strategy is the wideband RCS reduction for both polarizations. However, the performance is very sensitive to the angle of the incident wave. In [10–12], based on coding metasurface, the monostatic and bistatic

Received 28 March 2021, Accepted 16 August 2021, Scheduled 20 August 2021

* Corresponding author: Zengrui Li (zrli@cuc.edu.cn).

[1] Beijing Polytechnic, Beijing 100176, China. [2] State Key Laboratory of Media Convergence and Communication and the School of Information and Communication Engineering, Communication University of China, Beijing 100024, China.

RCSs of antennas can be reduced simultaneously. However, in the design of the coding units, the effect of the reflection characteristics of the antenna itself is ignored. A patch antenna array by using a 1-D periodic metasurface with low scattering performance in band is designed, which obtains more than 5 dB RCS reduction over the array operating frequency band of 11.45% in [13]. By loading the randomized phase-encoded polarization conversion metasurface around a microstrip antenna in [14], low monostatic and bistatic RCS signatures are achieved out-of-band of the antenna in a frequency region from 8.2 to 25.6 GHz. In [15], a microstrip phased-array antenna with an integrated 2-bit phase shifter with low RCS characteristics at the single frequency based on randomly rotated array element is designed. In [16], an anisotropic metasurface is employed to replace the traditional patch and behaves as a radiating structure directly, which forms a 4×4 array and achieves RCS reduction in the resonant frequency of 3.05 GHz. By adding the metamaterial absorbers, the narrow bandwidth array antennas with both low scattering and good radiation properties are proposed in [17, 18].

In this paper, based on the principle of passive cancelation, an aperiodic configuration of AMCs is applied to reduce both monostatic and bistatic RCSs of the microstrip antenna array in a wide band. During the process, reflection characteristics of the microstrip antenna array are also taken into consideration. All AMC lattices are arranged in random order to minimize the maximum value of bistatic RCS. The microstrip antenna array is fabricated and measured, which shows that the relative bandwidth of 10 dB monostatic RCS reduction is about 79% (15.2–35 GHz). Meanwhile, compared with the regular chessboard configuration, the maximum bistatic RCS is reduced by about 4 dB, validating the feasibility of this scheme for effectively reducing both monostatic and bistatic RCS of the microstrip antenna array.

2. DESIGN AND ANALYSIS OF THE TRADITIONAL CHESSBOARD STRUCTURE

The microstrip antenna array, whose operation band is 20–20.75 GHz, is designed on a Rogers RT/duroid 5880 substrate with a relative permittivity of 2.2 and a loss tangent of 0.008, as well as a thickness of 0.5 mm and an overall size of $56 \times 56\,\text{mm}^2$. The array that consists of 4×4 antenna units is excited with the same amplitude and phase, while it is fed by a microstrip feed network printed on the substrate, as shown in Fig. 1. The characteristic impedance of one antenna unit is $100\,\Omega$. Through three times impedance conversion, the characteristic impedance of the lumped port is $50\,\Omega$.

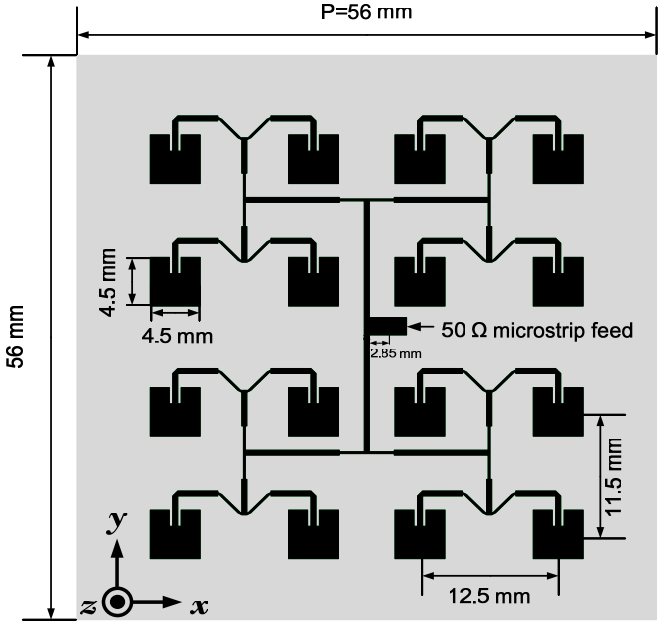

Figure 1. Configuration and parameters of the microstrip antenna array.

2.1. Design of the AMC Unit Cell

To reduce the RCS of antenna array, two Koch fractal patches with different dimensions are used as the AMC unit cells. The two unit cells are also constructed on a Rogers RT/duroid 5880 substrate with a thickness of 1.5 mm. All of the simulations are done using the full-wave simulator CST Microwave Studio® 2019 software [19].

As shown in Fig. 2, to satisfy the periodic boundary condition approximately, a lattice containing 8×8 identical unit cells is generated. The period of all AMC unit cells is $L = 3.5$ mm. Based on the principle of passive cancelation, AMC#1 with $a = 0.5$ mm and AMC#2 with $a = 3.15$ mm are specially selected in order to achieve a relatively constant phase difference of reflection coefficient (nearly 180°) in a wide range of frequencies at normal incidence, which covers the operating frequency of the microstrip antenna array.

To analyze the scattering performance of the two AMC unit cells, each of AMC structures has been independently simulated. Fig. 3 depicts that the reflection phase of AMC#1 and AMC#2 can retain a

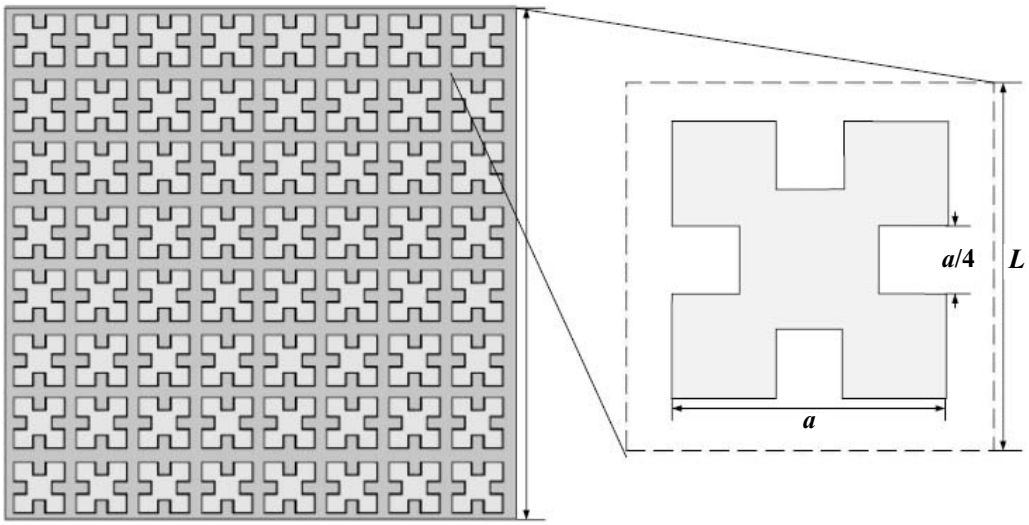

Figure 2. AMC lattice and unit cell.

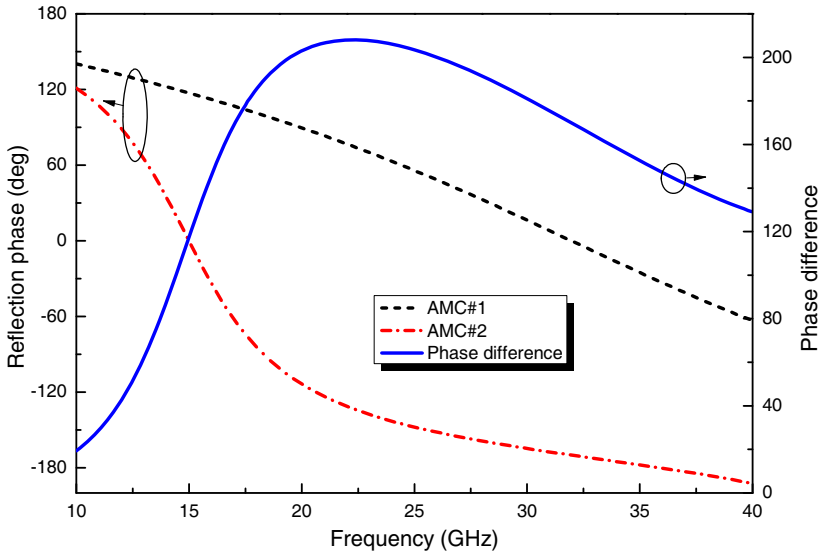

Figure 3. Reflection phase of AMC#1, AMC#2 and phase difference as a function of frequency.

180° (±37°) of phase shift from 16 to 36.5 GHz when the incident wave is perpendicular to the ground plane of the AMCs.

2.2. Design of the Traditional Chessboard Structure

We choose AMC#1 and AMC#2 as the basic units for the design of the traditional chessboard structure. As shown in Fig. 4, each row is arranged alternately by AMC#1 and AMC#2 lattices, while the antenna array is placed in the center. Fig. 5 shows the simulated monostatic RCS reduction of the antenna array with AMC structures (black dash line) for normal x-polarised incident wave. The model being compared is the same antenna array located in a metallic plate, while the metallic plate possesses the same dimensions as the AMC structures. It can be seen that the monostatic RCS reduction does not meet the requirement of −10 dB in the range of 19.5 to 27.5 GHz. The scattering pattern of the chessboard structure in 17.5 GHz is presented in Fig. 6.

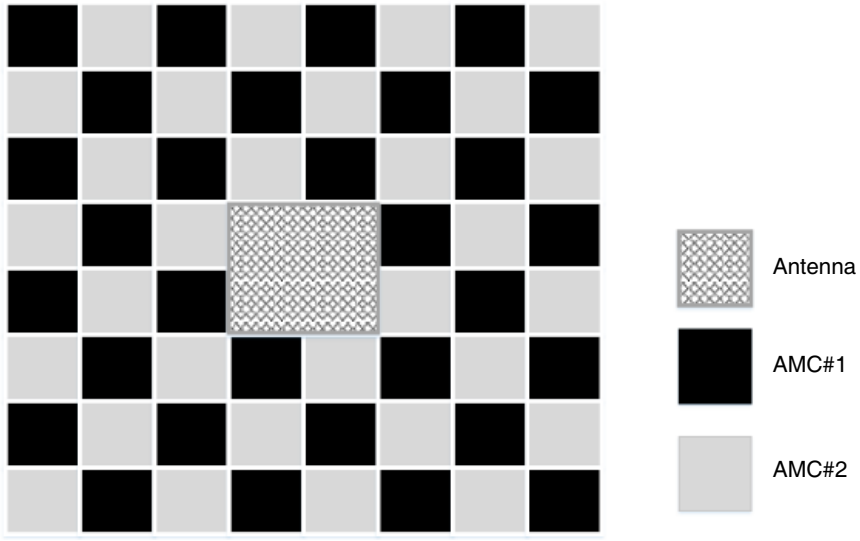

Figure 4. Configuration of the chessboard structure.

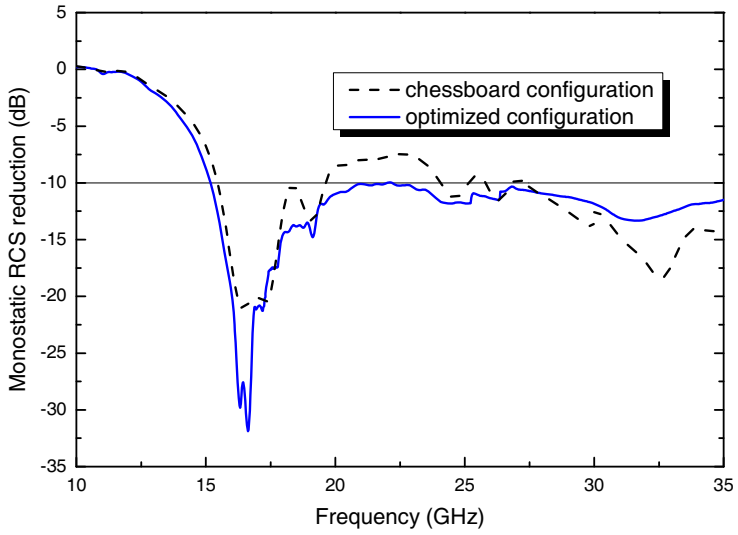

Figure 5. Simulation results of monostatic RCS for the antenna array with traditional chessboard structure or optimized aperiodic structure.

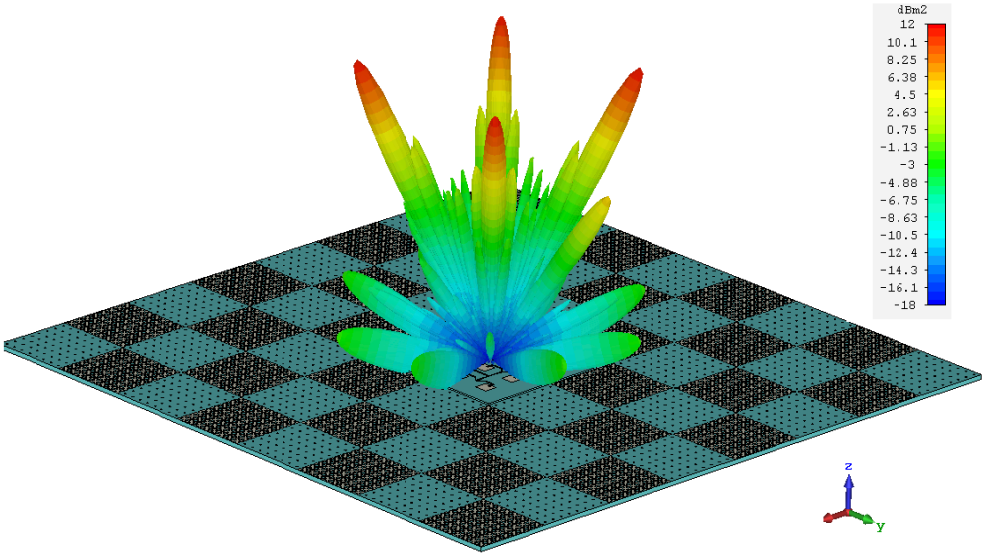

Figure 6. The scattering pattern of the chessboard structure.

3. RCS REDUCTION OF THE MICROSTRIP ANTENNA ARRAY

The microstrip antenna array contains of 16 radiation elements excited with same amplitude and phase, meanwhile it is fed by a microstrip feed network printed on the substrate. In order to obtain a wideband RCS reduction, we select new lattices to cancel out the reflection energy of scattering fields generated by the antenna itself. The other limitation of the periodic structure is that the scattered wave at normal incidence is redirected into four directions which may lead to an increase of bistatic RCS. This limitation can be overcome by substituting the periodic structure by the structure of aperiodic distribution. When AMCs are properly placed, the scattered wave can be suppressed in all directions.

In particular, we treat the microstrip antenna array as a new AMC unit cell (AMC#ANT), and the reflection performance at normal incidence is also simulated using a boundary conditions of periodic

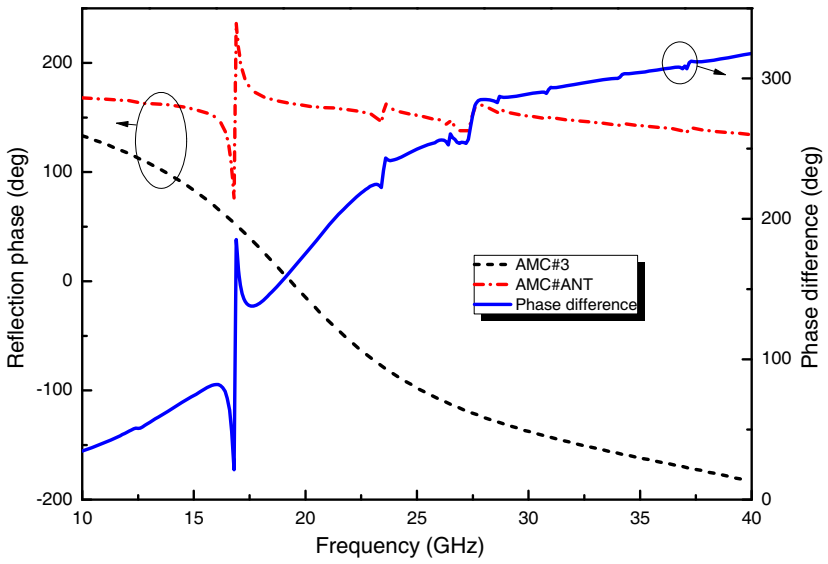

Figure 7. Reflection phase of AMC#3, AMC#ANT and phase difference between them as a function of frequency.

$P = 56\,\text{mm}$. In a similar way, another AMC unit cell (AMC#3) with the same structure as AMC#1 and boundary conditions is selected to achieve 180° (±37°) of phase shift with AMC#ANT in a wide range of frequencies. The physical dimension of AMC#3 is $a = 2.5\,\text{mm}$. The reflection phases of AMC#3 and AMC#ANT versus frequency, as well as the phase difference between them, are plotted in Fig. 7. In other words, three AMCs with different dimensions have been properly selected to compose the aperiodic configuration lattices to reduce the RCS in our design.

The combination of theoretical and numerical simulations is used to optimize the location of each lattice. This structure is modeled as an array of antennas based on array theory, and each element is excited with the same amplitude, meanwhile the phase of elements is obtained by CST simulation. As can be seen in Fig. 8, the aperiodic configuration consists of twenty-eight AMC#1 lattices, twenty-eight AMC#2 lattices, and four AMC#3 lattices.

To further illustrate the monostatic and bistatic RCS behavior of the antenna with aperiodic AMCs, this structure is simulated using the transient solver of CST Microwave Studio. Fig. 5 shows the

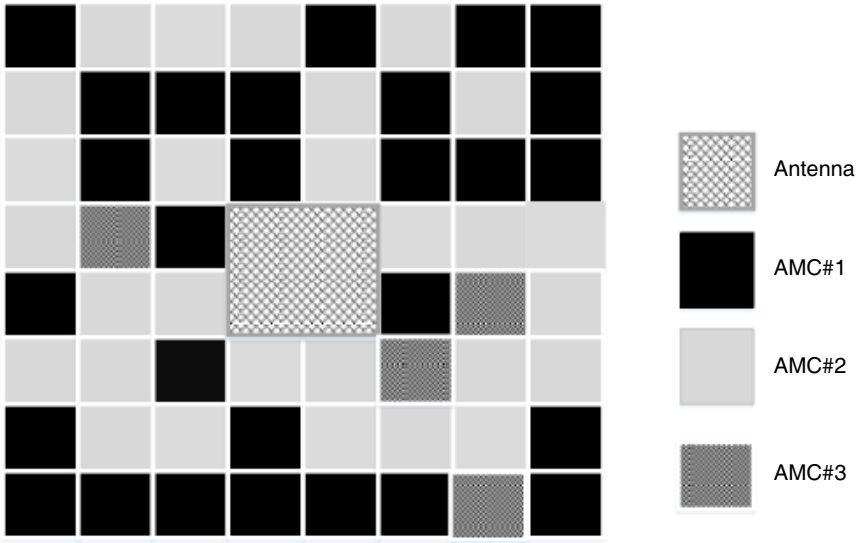

Figure 8. Configuration of the aperiodic structure.

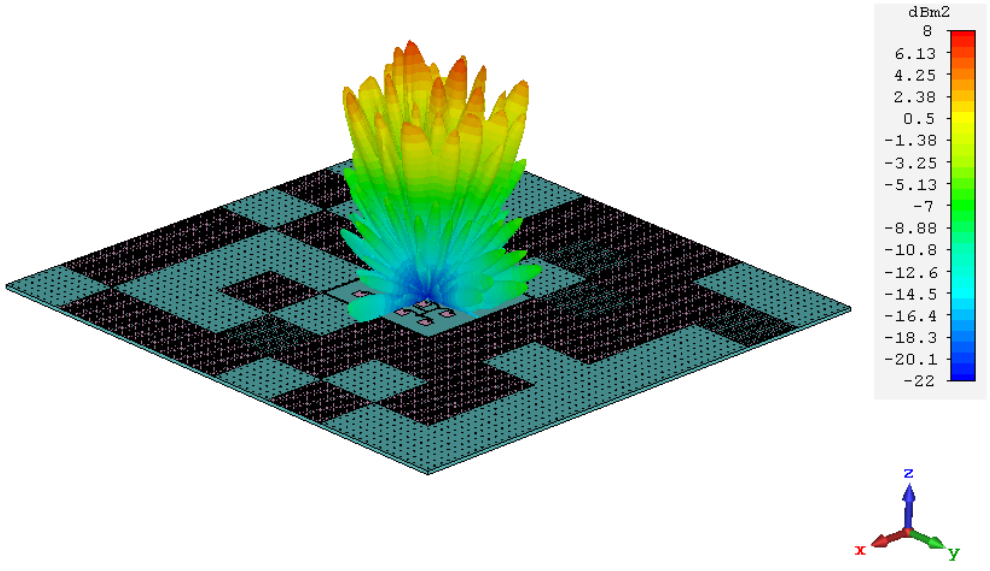

Figure 9. The scattering pattern of the optimized aperiodic structure.

simulated monostatic RCS of the antenna (blue solid line). The 3D RCS of the antenna with aperiodic AMCs for normal incidence at 17.5 GHz is presented in Fig. 9. As it is illustrated, scattered energy is evenly dispersed in all directions, and it will not increase bistatic RCS in either direction.

4. MEASUREMENT RESULTS

The proposed antenna was realized and measured. A photograph of the manufactured antenna with AMCs is shown in Fig. 10, while the measurements were taken in an anechoic chamber using the Agilent 8057 ENA series network analyzer. The simulated and measured results of reflection coefficient of the antenna with aperiodic AMCs are shown in Fig. 11, while the measured result agrees with the simulated one. The normalized radiation patterns in the E and H planes at 20.5 GHz were simulated and measured. As shown in Fig. 12 and Fig. 13, the measured normalized radiation patterns (mea) agree well with the simulated results (sim). A high-precision RCS measurement is conducted using a compact antenna test range system, and the entire measurement band ranges from 10 to 35 GHz, which covers four pairs of standard linearly polarized horn antennas operating at 8–12, 12–18, 18–26.5, and 26.5–40,

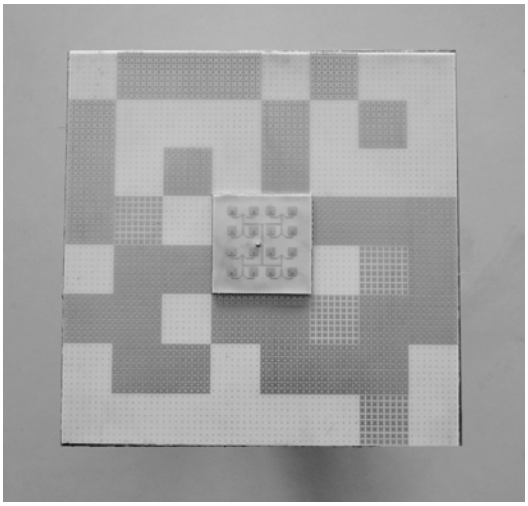

Figure 10. Photograph of the proposed antenna with AMCs.

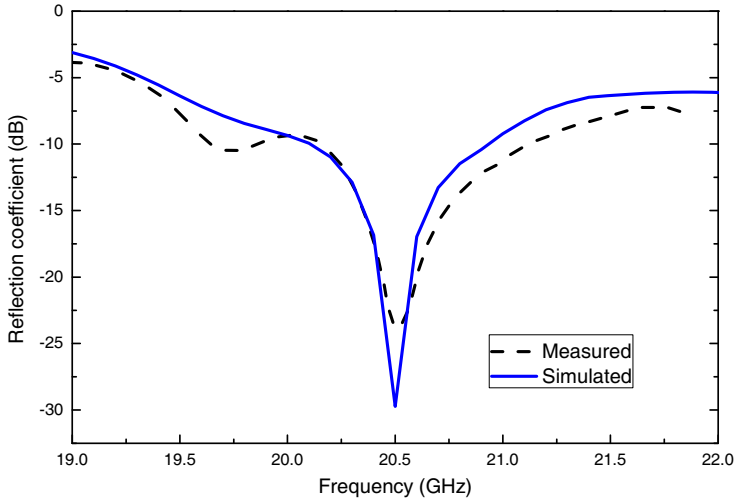

Figure 11. Simulated and measured results of reflection coefficient.

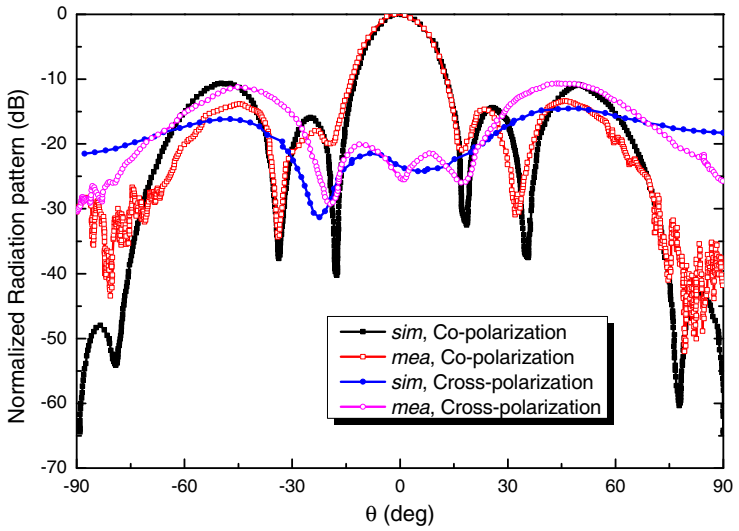

Figure 12. Simulated and measured results of normalized radiation patterns in the E plane.

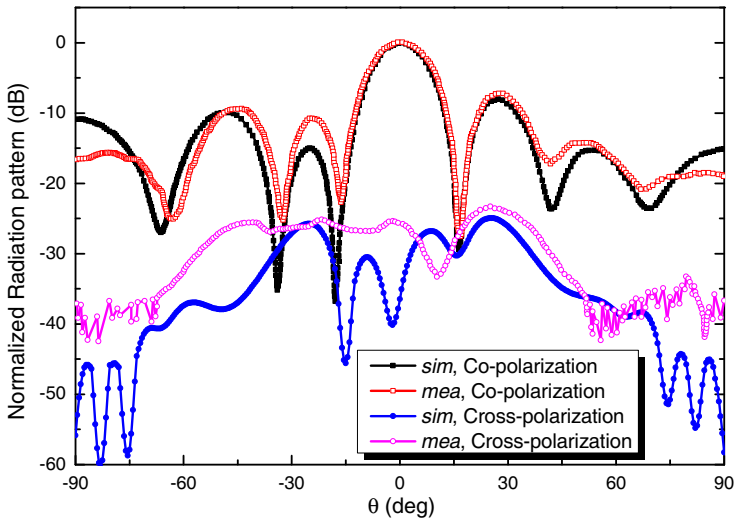

Figure 13. Simulated and measured results of normalized radiation patterns in the H plane.

Table 1. Comparison of the performance between the previous reported low-RCS antenna arrays and this work.

Reference	Impendance BW (GHz)	RCS reduction (dB)	OFB (GHz)	FBW (%)
[14]	N/A	10	8.2–25.6	102
[20]	2.99–3.16	10	8.5–11.5	30
[21]	9.85–10.1	10	5.1–9.5	60.2
[22]	10.1–11.6	6	6.2–15.2	84
[23]	26.7–34.2	10	28–47.7	52
This work	20–20.75	10	15.2–35	79

respectively. The RCSs of the antenna and equal-sized copper ground of the proposed metasurface are separately measured, and subtraction is made to obtain the RCS reduction. Fig. 14 shows the simulated and measured results of monostatic RCS reduction. An ultra-wideband RCS reduction larger than 10 dB is achieved in the frequency range from 15.2 to 35 GHz for x-polarised incident wave. A comparison of the impendence bandwidth (BW), operating frequency band (OFB), fractional bandwidth (FBW) of the RCS reduction between the previous studies and this paper is provided in Table 1. Obviously, our work has advantage in the bandwidth expansion of RCS reduction, and diffusion scattering is also realized for the microstrip antenna array.

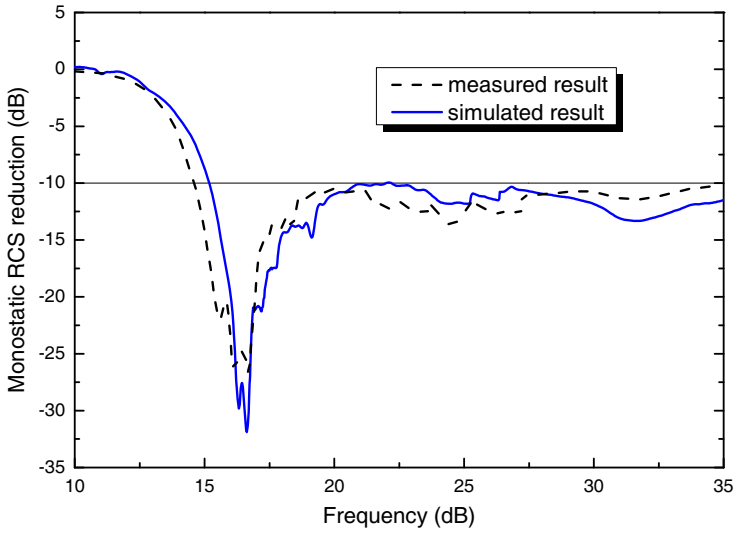

Figure 14. Simulated and measured results of monostatic RCS reduction.

5. CONCLUSION

In this work, to reduce the RCS of the microstrip antenna array, the designs, simulations, and measurements of the aperiodic structure with Koch fractal AMC lattices are presented and discussed. In particular, the reflection characteristics of the microstrip antenna array are also taken into consideration during the design process, while the lattices are randomly distributed to have a better behavior in bistatic RCS reduction. The experiment results demonstrate the validity of the proposed approach and suggested structure. Measurements and simulations show that by employing AMCs, 10 dB RCS reduction is achieved from 15.2 GHz to 35 GHz (about 79% relative bandwidth) without compromising the radiation characteristics of the antenna array.

REFERENCES

1. Genovesi, S., F. Costa, and A. Monorchio, "Low-profile array with reduced radar cross section by using hybrid frequency selective surfaces," *IEEE Transactions on Antennas and Propagation*, Vol. 60, No. 5, 2327–2335, May 2012.
2. Jia, Y., Y. Liu, H. Wang, and S. Gong, "Low RCS microstrip antenna using polarization-dependent frequency selective surface," *Electronics Letters*, Vol. 50, 978–979, Jul. 2014.
3. Joozdani, M. Z., M. K. Amirhosseini, and A. Abdolali, "Wideband radar cross-section reduction of patch array antenna with miniaturized hexagonal loop frequency selective surface," *Electronics Letters*, Vol. 52, No. 9, 767–768, Apr. 2016.
4. Paquay, M., J. C. Iriarte, I. Ederra, et al., "Thin AMC structure for radar cross-section reduction," *IEEE Transactions on Antennas and Propagation*, Vol. 55, No. 12, 3630–3638, Dec. 2007.

5. Galarregui, J. C. I., A. T. Pereda, J. L. M. de Falcon, et al., "Broadband radar cross-section reduction using AMC technology," *IEEE Transactions on Antennas and Propagation*, Vol. 61, No. 12, 6136–6143, Dec. 2013.
6. Esmaeli, S. H. and S. H. Sedighy, "Wideband radar cross-section reduction by AMC," *Electronics Letters*, Vol. 52, No. 1, 70–71, Jan. 2016.
7. Su, J., Y. Lu, H. Zhang, et al., "Ultra-wideband, wide angle and polarization-insensitive specular reflection reduction by metasurface based on parameter-adjustable meta-atoms," *Scientific Reports*, 11 pages, Feb. 2017.
8. Liu, Y., Y. Hao, K. Li, et al., "Radar cross section reduction of a microstrip based on polarization conversion," *IEEE Antennas and Wireless Propagation Letters*, Vol. 15, 80–83, 2016.
9. Liu, Y., K. Li, Y. Jia, et al., "Wideband RCS reduction of a slot array antenna using polarization conversion metasurfaces polarization conversion metasurfaces," *IEEE Transactions on Antennas and Propagation*, Vol. 64, No. 1, 326–331, 2016.
10. Su, J., C. Kong, Z. Li, et al., "Wideband diffuse scattering and RCS reduction of microstrip antenna array based on coding metasurface," *Electronics Letters*, Vol. 53, No. 16, 1088–1090, Aug. 2017.
11. Su, J., H. He, Z. Li, et al., "Uneven-layered coding metamaterial tile for ultra-wideband RCS reduction and diffuse scattering," *Scientific Reports*, 9 pages, May 2018.
12. Liu, X., J. Gao, L. Xu, et al., "A coding diffuse metasurface for RCS reduction," *IEEE Antennas and Wireless Propagation Letters*, Vol. 16, 724–727, 2017.
13. Han, Z., W. Song, and X. Sheng, "In-band RCS reduction and gain enhancement for a patch antenna array by using a 1-D periodic metasurface reflector," *IEEE Transactions on Antennas and Propagation*, Vol. 67, No. 6, 4269–4274, Jun. 2019.
14. Rajabalipanah, H. and A. Abdolali, "Ultrabroadband monostatic/bistatic RCS reduction via high-entropy phase-encoded polarization conversion metasurfaces," *IEEE Antennas and Wireless Propagation Letters*, Vol. 18, No. 6, 1233–1237, Jun. 2019.
15. Yin, L., P. Yang, Y.-Y. Gan, F. Yang, S. Yang, and Z. Nie, "A low cost, low in-band RCS microstrip phased-array antenna with integrated 2-bit phase shifter," *IEEE Transactions on Antennas and Propagation*, 2020.
16. Yang, H., et al., "Low in-band-RCS antennas based on anisotropic metasurface using a novel integration method," *IEEE Transactions on Antennas and Propagation*, Vol. 69, No. 3, 1239–1248, Mar. 2021.
17. Han, Y., S. Gong, J. Wang, Y. Li, S. Qu, and J. Zhang, "Reducing RCS of patch antennas via dispersion engineering of metamaterial absorbers," *IEEE Transactions on Antennas and Propagation*, Vol. 68, No. 3, 1419–1425, Mar. 2020.
18. Han, Y., L. Zhu, Y. Bo, W. Che, and B. Li, "Novel low-RCS circularly polarized antenna arrays via frequency-selective absorber," *IEEE Transactions on Antennas and Propagation*, Vol. 68, No. 1, 287–296, Jan. 2020.
19. CST STUDIO SUITE®, CST AG, Germany, www.cst.com.
20. Zhang, C., J. Gao, X. Cao, L. Xu, and J. Han, "Low scattering microstrip antenna array using coding artificial magnetic conductor ground," *IEEE Antennas and Wireless Propagation Letters*, Vol. 17, No. 5, 869–872, May 2018, doi: 10.1109/LAWP.2018.2820220.
21. Chen, Q., M. Guo, D. Sang, Z. Sun, and Y. Fu, "RCS reduction of patch array antenna using anisotropic resistive metasurface," *IEEE Antennas and Wireless Propagation Letters*, Vol. 18, No. 6, 1223–1227, Jun. 2019, doi: 10.1109/LAWP.2019.2913104.
22. Cheng, Y.-F., C. Liao, G. -F. Gao, L. Peng, and X. Ding, "Performance enhancement of a planar slot phased array by using dual-mode SIW cavity and coding metasurface," *IEEE Transactions on Antennas and Propagation*, 2021.
23. Zarbakhsh, S., M. Akbari, F. Samadi, and A. Sebak, "Broadband and high-gain circularly-polarized antenna with low RCS," *IEEE Transactions on Antennas and Propagation*, Vol. 67, No. 1, 16–23, Jan. 2019.